Epilepsia, **49**(Suppl. 2):33–41, 2008
doi: 10.1111/j.1528-1167.2008.01491.x

Rapid astrocyte and microglial activation following pilocarpine-induced seizures in rats

Lee A. Shapiro, Lulu Wang, and Charles E. Ribak

Department of Anatomy & Neurobiology, School of Medicine, University of California at Irvine, Irvine, California, U.S.A.

SUMMARY

Astrocyte and microglial activation occurs following seizures and plays a role in epileptogenesis. However, the precise temporal and spatial response to seizures has not been fully examined. The pilocarpine model of temporal lobe epilepsy was selected to examine glial changes following seizures because morphological changes in the hippocampus closely mimic the human condition. Astrocytic and microglial changes in the hippocampus were examined during the first 5 days after pilocarpine-induced seizures in rats by analyzing GFAP, Iba1 and S100B-immunolabeling in CA1, CA3, and the hilus. Also, 3-dimensional reconstructions of microglial cells from the hilus and granule cell layer were analyzed. Lastly, astrocyte hypertrophy was examined in the hilus using electron microscopy. At 1 day after seizures and continuing throughout the 5 days examined, hypertrophied Iba1-labeled microglial cells and glial fibrillary acidic protein (GFAP)-labeled astrocytes were observed. At 1 and 2 days after seizures, significantly greater Iba1 immunolabeling was observed in CA1, CA3, and the hilus. In addition, both the area of Iba1 labeled processes and the number of their endings were increased in the hilus beginning at 1 day after seizures. S100B-immunolabeling was significantly elevated in CA3 at 1 day, in CA3 and CA1 at 2 days, and in all three hippocampal regions at 3 days after seizures. Electron microscopy confirmed astrocytic hypertrophy and demonstrated astrocytic cell bodies in the location where glial endfeet normally appear on capillaries. The differential response patterns of astrocytes and microglial cells following pilocarpine-induced seizures may signify their detrimental role in neuroinflammation after seizures.

KEY WORDS: **Temporal lobe epilepsy, Dentate gyrus, Hippocampus, Astrocyte hypertrophy, Glial filaments.**

Astrocyte and microglial activation are well-described features of temporal lobe epilepsy (TLE), and studies have suggested that glial cells may contribute to epileptogenesis (Briellmann et al., 2002; Vessal et al., 2005; Kang et al., 2006; Binder & Steinhäuser, 2006). Other studies have shown that after seizures, hypertrophied astrocytes in the dentate gyrus form an ectopic glial scaffold that promotes the aberrant growth of basal dendrites into the hilus (Shapiro et al., 2005a; Shapiro & Ribak, 2006). These basal dendrites are targeted for synaptogenesis by mossy fibers (Ribak et al., 2000; Shapiro & Ribak, 2006) and contribute to a recurrent excitatory circuit that may facilitate seizures (Austin & Buckmaster, 2004). While astrocyte and microglial activation might play a role in facilitating the subsequent appearance of spontaneous seizures, the process of glial activation is complex, and the precise temporal and spatial sequelae of the neuroinflammatory response following seizures are not well-studied (Borges et al., 2003).

The rodent-pilocarpine model of TLE is commonly used to examine the neuroplastic changes that occur in the epileptic brain, including mossy fiber sprouting (Mello et al., 1993; Buckmaster et al., 2002), cell death (Mello et al., 1993), increased neurogenesis (Parent et al., 1997; McCloskey et al., 2006) and persistent basal dendrites that receive mossy fiber synapses in the hilus (Ribak et al., 2000; Shapiro & Ribak, 2006). These changes were initially described at 30 days after pilocarpine-induced seizures, a time point after the onset of spontaneous seizures. More recently, similar neuroplastic changes have been shown to occur within the first 5 days after pilocarpine-induced seizures (Shapiro et al.,

Address correspondence to Dr. Charles E. Ribak, Department of Anatomy and Neurobiology, School of Medicine, University of California at Irvine, Irvine, CA 92697-1275. E-mail: ribak@uci.edu

Blackwell Publishing, Inc.

2007a). Considering that neuroplastic changes occur immediately following the seizures, and that astrocyte activation might contribute to the epileptogenic condition (Niquet et al., 1994; Briellmann et al., 2002; Drage et al., 2002; Garzillo & Mello, 2002; Vessal et al., 2005; Kang et al., 2006; Binder & Steinhäuser, 2006), the current study was designed to define the progression of astrocyte and microglial activation at 1–5 days after pilocarpine-induced seizures. This was accomplished using an immunocytochemical analysis of astrocytes and microglial cells labeled with antibodies for glial fibrillary acidic protein (GFAP) and Iba1, respectively.

In addition to these two glial cell types, S100B-labeled astrocytes were also examined. S100B has been shown to be involved in the neuroinflammatory response to many neuropathological conditions (Griffin et al., 1989; Li et al., 2000), including human TLE (Griffin et al., 1995). Antibodies to the S100B protein can be used to assess varying degrees of neuroinflammation (Rothermundt et al., 2003). There are reports showing that S100B is involved with intermediate glial filament assembly and disassembly, as well as polymerization of GFAP (Selinfreund et al., 1991; Bianchi et al., 1996; Ueda et al., 1994). Moreover, S100B stimulates microglial cell activation (Yan et al., 1996; Sheng et al., 1997) and S100B expression is increased 30 days after kainate-induced lesions (Bendotti et al., 2000). Therefore, the distribution of S100B-labeled cells was mapped throughout the hippocampus at 1–5 days after pilocarpine-induced seizures.

Comparisons between the control group and each of the time points following pilocarpine administration were performed on the levels of immunoreaction product for each antibody. Moreover, the morphology of Iba1-labeled microglial cells was characterized by tracing 3-D reconstructions, and an analysis was performed to compare process thickness and branching patterns in response to seizure activity. Lastly, electron microscopy was used to examine astrocytic hypertrophy following seizures.

METHODS

Animals

Adult male Sprague-Dawley rats (N = 24) were used for this study. All protocols and experiments were carried out in accordance with the Institutional Animal Care and Use Committee at the University of California, Irvine. Pilocarpine (320–340 mg/kg, i.p.) was used to induce seizures as previously described (Shapiro et al., 2007a). At the appropriate time points after seizures, the rats were deeply anesthetized with euthasol and transcardial perfusions were carried out using 250 ml of 0.9% sterile saline, followed by 4.0% paraformaldehyde. The brains were allowed to postfix in the skull for 24 h, after which they were dissected out and placed in 4.0% paraformaldehyde for 24 h. The brains were then transferred to phosphate-buffered saline (PBS) and 50 μm sections were cut using a vibratome.

Immunohistochemistry

Sections used for immunocytochemistry were 50 μm in thickness and were incubated in 0.5% H_2O_2 for 30 min, followed by 60 min in 1% H_2O_2, and then again for 30 min in 0.5% H_2O_2. Sections were then rinsed with PBS and incubated free-floating in anti-GFAP (1:1000, Sigma, St Louis, MO, U.S.A.), Iba1 (1:1000, Wako, Osaka, Japan), or S100B (1:1000, Sigma), with 3% normal goat serum, 0.05% Triton-X in PBS, for 24 h rotating at room temperature (RT). The tissue was then rinsed 3 times for 5 min in PBS and incubated for 1 h in biotinylated anti-rabbit (GFAP and Iba1; 1:200, Vector Labs, Burlingame, CA, U.S.A.), or anti-mouse (S100B; 1:200, Vector Labs Burlingame, CA, U.S.A.) IgG, rotating at RT. For fluorescent staining, the tissue was incubated for 1.5 h in fluorescent-tagged anti-rabbit (GFAP and Iba1; 1:200, Molecular Probes, Carlsbad, CA, U.S.A.) or anti-mouse (S100B; 1:200, Molecular Probes) IgG, rotating at RT. For diaminobenzidine (DAB) stained sections, the tissue was then rinsed in PBS 3 times for 5 min each rinse, and incubated for 1 h in ABC (Vector Labs) solution, rotating at RT. Following incubation, sections were rinsed with PBS for 20 min and were developed by incubating in 0.025% DAB and 0.002% hydrogen peroxide, in PBS. The DAB reaction was halted using PBS, followed by three 10 min PBS rinses, after which the tissue was mounted onto glass slides, dehydrated in graded alcohol baths, and coverslips were applied using Permount (Sigma). For fluorescent reactions, the tissue was rinsed in PBS following the secondary reaction, mounted in distilled water, and coverslips were applied using Fluoromount-G (Southern Biotech, Birmingham, AL, U.S.A.).

Image analysis

Distribution of astrocytes and microglial cells following pilocarpine-induced seizures

The distribution, size, and morphology of the three immunolabeled cell types were plotted onto schematic diagrams of the hippocampus by a rater blind to the condition of the rats. At each of the time points examined (N = 4/time point) and in the control (N = 4), a minimum of 12 sections containing the hippocampus was examined from each group.

Analysis of astroglial and microglial activation within regions of the hippocampus

The magnitude of astroglial and microglial immunoreactivity was measured using a computer-assisted image analysis program (The University of Texas ImageTool program V. 3.0). Sections containing GFAP, S100B, or Iba1 labeled glial cells were examined under a Zeiss light microscope (Zeiss Axioplan, Thornwood, NY, U.S.A.). Grayscale images (N = 24 per region examined, per time point) were

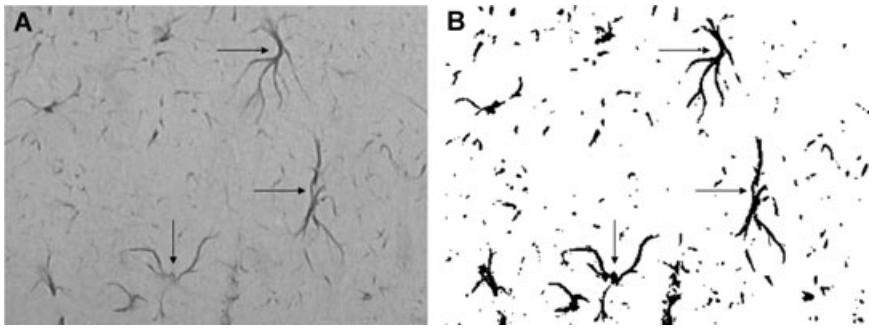

Figure 1.
Example of the densitometric method used to analyze immunolabeling in the hippocampus. In **A**, a light micrograph containing GFAP immunolabeled cells (arrows) and processes from 1 day after seizures is shown. In **B**, the same image is shown after digitally converting the image using the threshold feature of the ImageTool software (UTHSC). Only those immunolabeled elements that fall into the threshold range are converted to pure black pixels and the rest of the image is converted to pure white pixels. The software automates the analysis by quantifying the total number and percent of black and white pixels, allowing for statistical analysis of the data. Scale bars = 10 μm for **A** and **B**.

digitally captured from stratum radiatum of CA1 and CA3, as well as from the hilus of the dentate gyrus. A 300 μm^2 box was then randomly placed within the region of interest, and this area was used for analysis. The images were analyzed using the ImageTool (University of Texas Health Science Center) software which automates the analysis by converting all immunolabeled elements that fall within a threshold range into pure black pixels, and the rest of the image is converted into pure white pixels (see Fig. 1). The software then calculates the percentage of pure black and white pixels, allowing for the comparison of the pixel values between the groups using a one-way ANOVA. Planned-comparisons were carried out using the Bonferroni test.

3-D reconstructions of Iba1 labeled microglial cells

To determine the process area and branching patterns of the Iba1 expressing microglial cells, images were captured from the hilus (N = 12 cells per time point and 3 from the control) and dentate gyrus granule cell layer (GCL) (N = 8 cells per time point and 2 for the control). Confocal image stacks were captured as previously described (Shapiro et al., 2007b). The image stacks were then traced using the Stereo Investigator software (MicroBrightfield Inc., Williston, VT, U.S.A.), and a branched structure analysis was performed to examine the process length per cell, number of endings per cell (an indicator of ramification) and total process area. Total process area was examined because microglial hypertrophy typically involves a thickening, and not necessarily a lengthening, of the microglial processes. Statistical analysis of the data was performed using a one-way ANOVA, and planned-comparisons were carried out using the Bonferroni test.

Electron microscopy

Sections from the hippocampus were processed for electron microscopy using a previously described method (Shapiro & Ribak, 2006). Briefly, hippocampal sections were postfixed in 1% glutaraldehyde for 1 h, then rinsed in PBS and placed in 1% osmium tetroxide for 20–60 min, and dehydrated by ethanol and propylene oxide immersion. A flat-embedding procedure was used after which the tissue block was trimmed using a single-edged razor blade under a dissecting microscope. A short series of ultrathin (60–80 nm) sections containing the dentate gyrus from each block was cut with an ultramicrotome (UltraCut E, Reichert-Jung, Wetzlar, Germany), and sequential sections were collected on mesh and formvar-coated slot grids. The sections were stained with uranyl acetate and lead citrate to enhance contrast. Sections containing the GCL and hilus were examined with a Philips CM-10 transmission electron microscope, and images of astrocytic somata and processes were captured with a Gatan digital camera.

RESULTS

Distribution of glial cells in the hippocampus following pilocarpine-induced seizures

At 1 day after pilocarpine-induced seizures, hypertrophied GFAP-labeled astrocytes (Fig. 1) and Iba1-labeled microglial cells (Fig. 2) were seen throughout the hippocampal CA1 and CA3 regions, and in the dentate gyrus. Many of the Iba1-labeled cells at this time point were pleomorphic, with thickened processes and increased branchpoints, indicative of activated microglial cells. Interestingly, the Iba1 cells at the border between the subgranular zone and the base of the GCL were the most

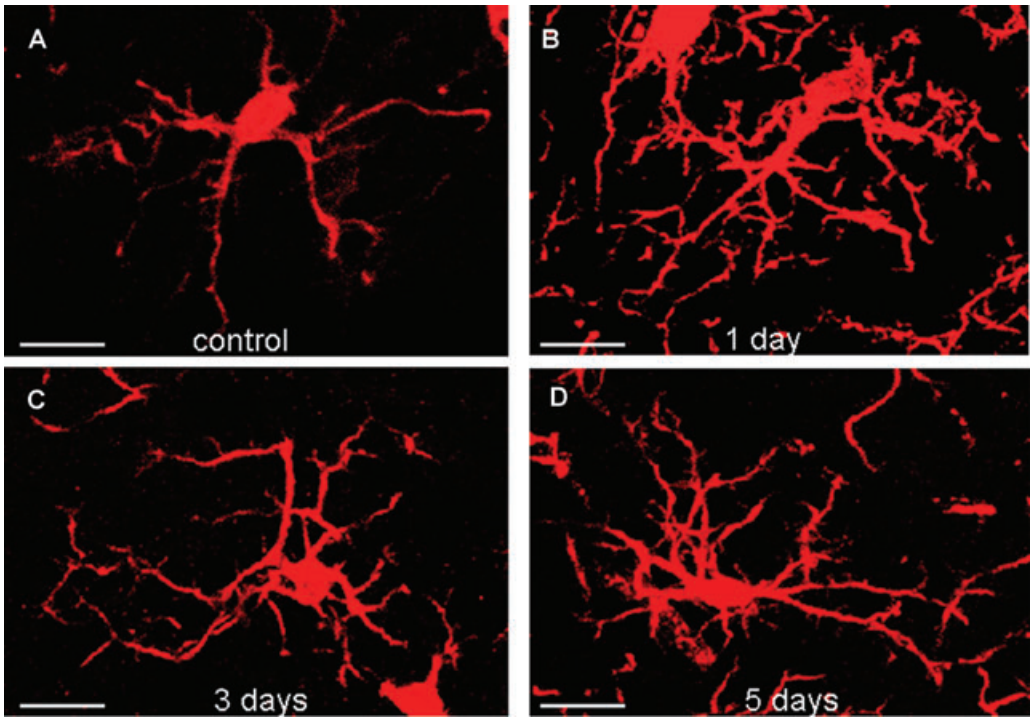

Figure 2.
Confocal micrographs of Iba1 labeled microglial cells in the hilus of the dentate gyrus from control (**A**) and epileptic rats (**B–D**). In **A**, an example of a labeled-cell is shown from the control. Note the typical resting microglial appearance with its round cell body (arrow) and normal appearing processes with relatively few ramifications. In **B**, a labeled microglial cell is shown at 1 day after pilocarpine-induced seizures. Note the activated appearance with its elongated cell body (arrow), thickened processes and increased number of branches. In **C**, a labeled microglial cell is shown at 3 days after seizures. Note that this cell still has an activated appearance. In **D**, a labeled microglial cell is shown at 5 days after seizures. Note that this cell also retains an activated appearance: indicating microglial activation for the duration of the examined time points. Scale bars = 10μm for **A-D**.

intensely immunolabeled and displayed bushy/ramified branching patterns. This population of Iba1-labeled microglial cells was not observed in the control rats. At the 1 day time point, there were relatively fewer GFAP-labeled cells compared to the control rats. However, GFAP-labeled astrocytes had a hypertrophied appearance with thickened processes. In addition, S100B-labeled glial cells were found that were surrounded by halos of S100B of varying intensity (not shown). This pattern of labeling for all three antibodies was similar at the 2 day time point. No compound granular corpuscles (aka Gitter cells) were observed within the first 2 days after seizures, indicating that necrosis was not yet complete. Beginning at 3 days and continuing at the 4 and 5 day time points, most of the Iba1 labeled microglial cells had an elliptical or elongated cell body and thickened processes relative to the control group. At the 3 day time point, the S100B cells appeared more intensely-labeled throughout the regions examined, and many of these cells had halos of S100B (not shown). At 4 days after seizures, a majority of the GFAP- and Iba1-labeled cells had a hypertrophied appearance. However, in contrast to the 1–3 day time points, there was a greater proportion of cells that lacked the hypertrophied appearance, and instead appeared more like that of the control rats. At 5 days after seizures, some GFAP- and Iba1-labeled cells still had an activated appearance, although greater than half of these cells appeared relatively normal. It is pertinent to note that several rod-like Iba1 labeled cells were found at this time point, indicating chronic activation of these microglial cells (Fig. 3). The majority of the S100B-labeled cells at the 5 day time point lacked the intense S100B labeling, and was similar in appearance to the control rats, although diffuse halos of S100B were still observed around some of these cells.

Morphometric analysis

Analysis of the 3-D reconstructions of Iba1 expressing microglial cells revealed several differences in the

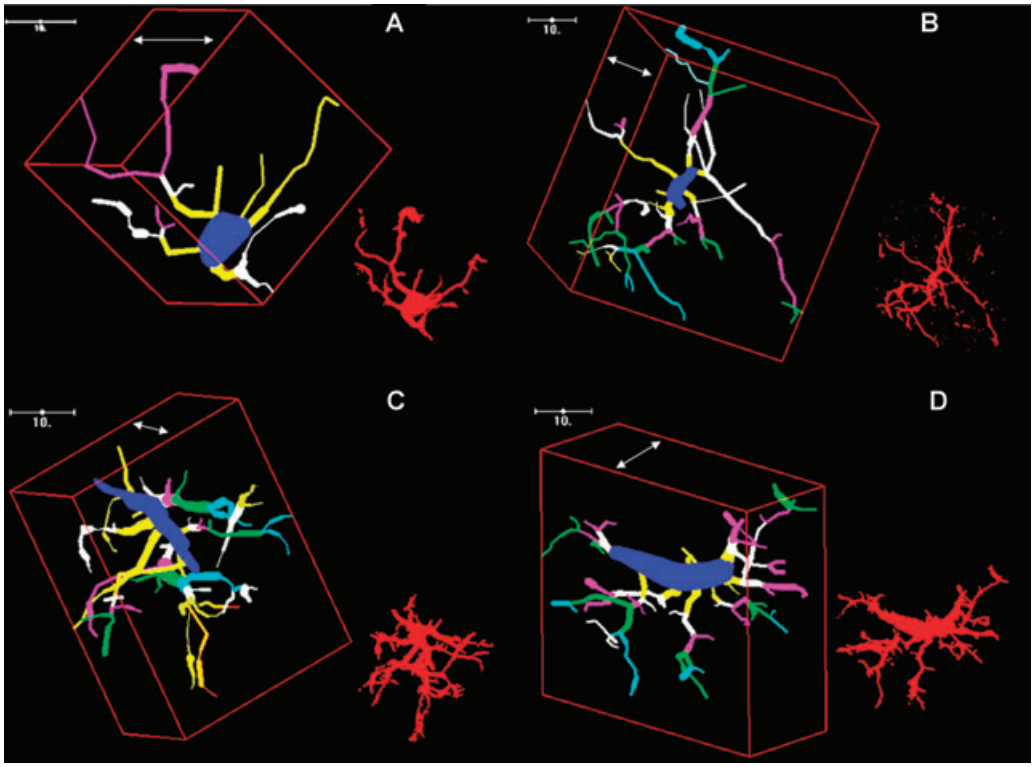

Figure 3.
3-D reconstructions of Iba1-labeled microglial cells in the hilus. The box enclosing the tracings depicts the x-, y-, and z-axes. The cell bodies of all cells are in blue, the first-order processes are in yellow, second-order processes are white, third order are magenta, fourth order are green, fifth order are light blue. The scale bars in each panel are for the traced cells, whereas the confocal images in the lower right of each panel are merged composites and are not to scale. In **A**, a typically appearing resting microglial cell is shown from the control group. In **B**, the microglial cell from 1 day after seizures has an elongated cell body (blue) with thickened processes and increased branching. In **C** (3 days), the cell body (blue) is more elongated and the processes are thick with complex ramifications. In **D** (5 days), the cell body (blue) appears rod-like with many short thickened processes emanating from the cell body. Scale bars = 10 μm.

morphology of the microglial cells between the control and experimental groups (Fig. 4). Although there were no differences in the mean length of Iba1 labeled processes between the controls and any of the rats that had experienced seizures, significant differences were detected in the mean area of these processes and number of their endings. The results showed a significantly greater area of Iba1 labeled processes in the hilus at 1 day ($p < 0.05$), 2 days ($p < 0.05$), 3 days ($p < 0.005$) and 5 days ($p < 0.001$) after seizures as compared to the control group. No significant differences were detected for the mean area of Iba1-labeled processes in the GCL at any of the time points examined (Fig. 4). Analysis of the mean number of endings of Iba1 labeled processes revealed a significantly greater number of endings in the hilus at day 1 ($p < 0.005$) and day 5 ($p < 0.001$) as compared to the control group. In the GCL, a significantly greater number of endings was found at day 1 ($p < 0.005$) as compared to the control group.

Densitometric analysis

The quantitative data for the densitometric analysis are shown in Fig. 5. At 1 day after seizures, there was increased Iba1 immunoreactivity relative to the control group in all three regions examined (hilus $p < 0.05$; CA1 $p < 0.001$; CA3 $p < 0.001$). There was also an increase in S100B immunoreactivity in CA3 ($p < 0.05$) at this time point. At 2 days after seizures, there was increased Iba1 immunoreactivity relative to the control group in all three regions examined (hilus $p < 0.01$; CA1 $p < 0.05$; CA3 $p < 0.005$). There was also an increase in S100B immunoreactivity in CA1 ($p < 0.05$) and CA3 ($p < 0.005$) at this time point. At 3 days after seizures, S100B immunoreactivity

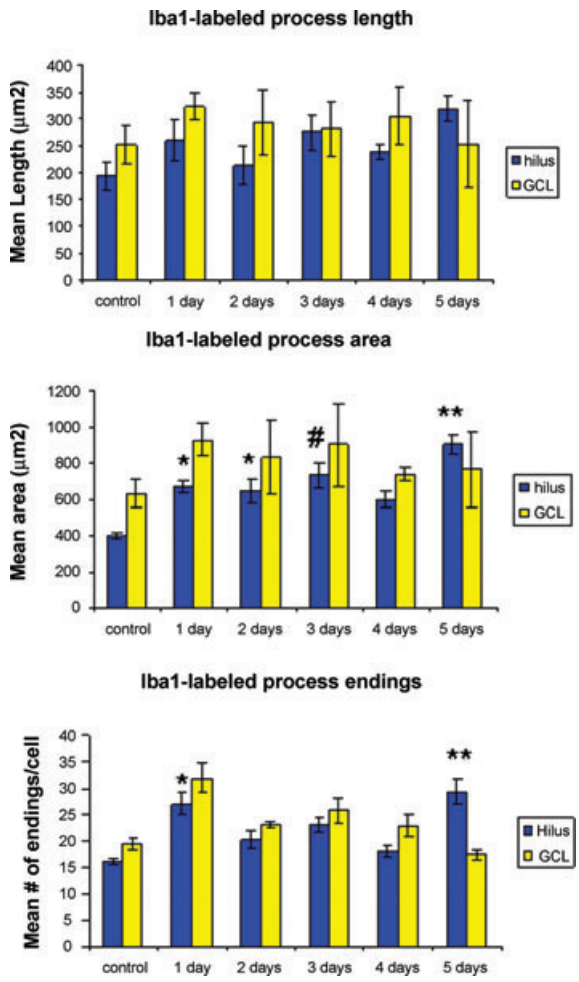

Figure 4.
Quantitative analysis of the mean length, number of process endings and mean process area of Iba1 labeled microglial cells in the hilus and granule cell layer (GCL). In **A**, the mean length is shown. One way analysis of variance did not reveal any significant differences at any of the time points examined. In **B**, the graph depicting the mean area of Iba1 labeled processes shows a significantly greater area in the hilus as compared to the control at 1 day ($^{*}p < 0.05$), 2 days ($^{*}p < 0.05$), 3 days ($p < 0.005$) and 5 days ($^{**}p < 0.001$) after seizures. In **C**, one way analysis of variance revealed significant differences in the mean number of Iba1 labeled endings in the hilus at 1 day ($^{*}p < 0.005$) and 5 days after seizures ($^{**}p < 0.001$) .
Epilepsia © ILAE

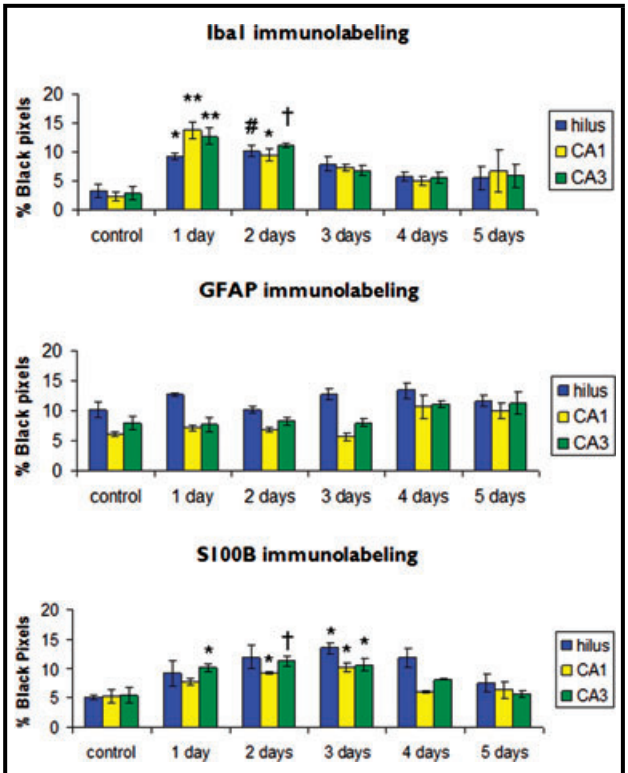

Figure 5.
Graphs of the mean percentage of black pixels for the Iba1, GFAP, and S100B immunocytochemical analysis. In **A**, the mean percentage of black pixels representing Iba1 labeling is shown. One way analysis of variance revealed that there is significantly greater immunoreactivity at 1 day (*hilus $p < 0.05$; CA1 and CA3 $^{**}p < 0.001$) and 2 days (hilus $p < 0.01$; CA1 $^{*}p < 0.05$; CA3 $\dagger p < 0.005$) after seizures relative to the controls in all of the regions examined. In **B**, the mean percentage of black pixels representing GFAP immunolabeling is shown. One way analysis of variance revealed no significant differences were detected at any of the time points examined. In **C**, the mean percentage of black pixels representing S100B immunoreactivity is shown. One way analysis of variance revealed that there is a significant increase in CA3 ($^{*}p < 0.05$) at 1 day, CA1 ($^{*}p < 0.05$) and CA3 ($\dagger p < 0.005$) at 2 days and in all three regions examined at 3 days ($^{*}p < 0.05$ for all three regions.
Epilepsia © ILAE

was increased relative to the controls in all of the regions examined ($p < 0.01$ for all three regions). GFAP immunolabeling showed no significant differences at any of the five time points following pilocarpine-induced seizures as compared to the control.

Electron microscopy of astrocyte hypertrophy

The control preparations of the hilus of the dentate gyrus showed the typical features of astrocytes (Shapiro et al., 2005b). The cell bodies of astrocytes were rarely found adjacent to the basal lamina of capillaries. Instead, the basal lamina was apposed by astrocytic endfeet, some of which were thin attenuated processes separating neuropil, while other processes were large and contained a watery

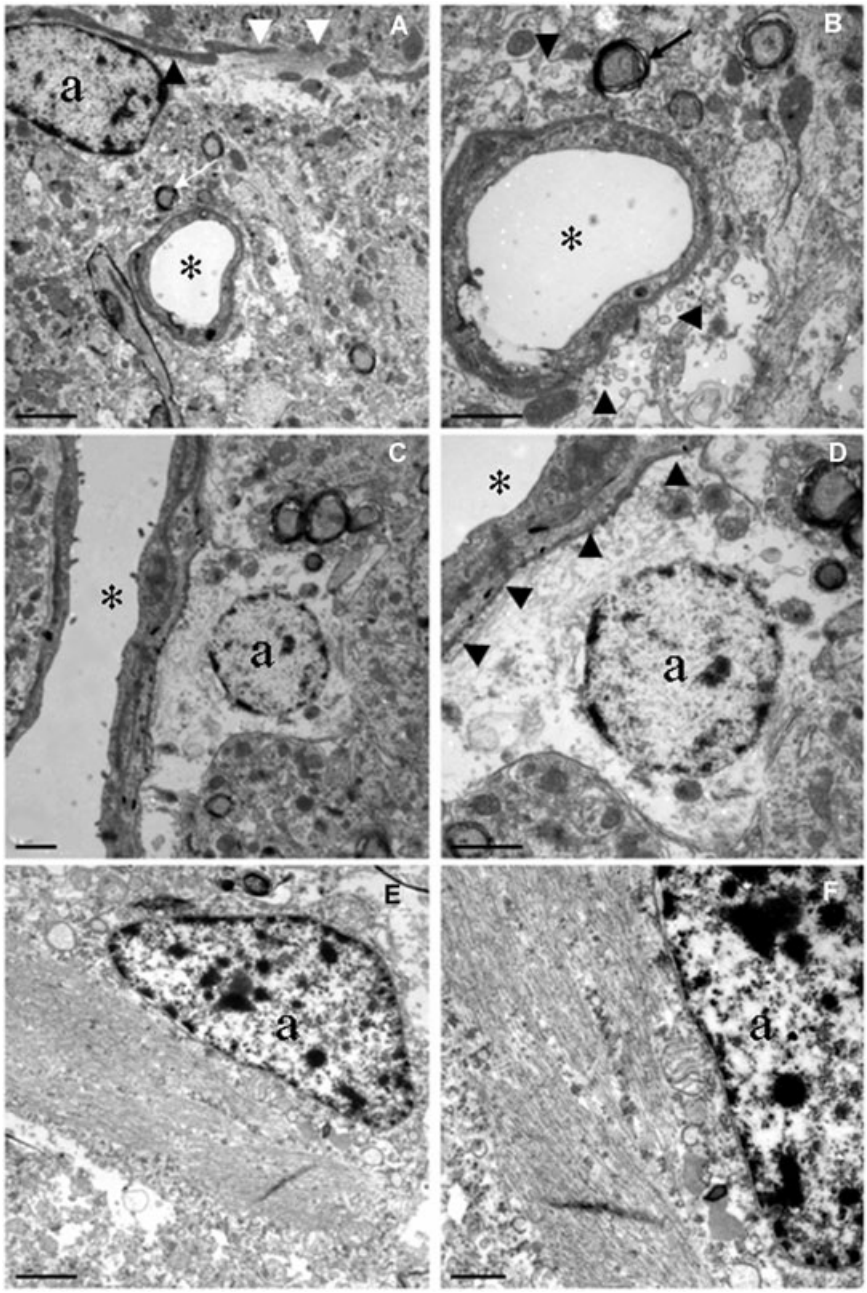

Figure 6.
Electron micrographs of astrocytes in the hilus of the dentate gyrus from control (**A, B**) and epileptic rats (**C–F**). **A** shows a low magnification of the subgranular zone with a capillary (asterisk) and a cell body of an astrocyte (a). Note the elongated mitochondria (black arrowhead) and bundles of glial filaments (white arrowheads) in the cytoplasm of the astrocyte cell body and proximal process. **B** is an enlargement of the capillary (asterisk) in **A**. Note that small profiles of glial endfeet separate the myelinated axon (arrow) from the basement lamina of this capillary. Another glial endfoot with vacuoles (black arrowheads) is shown on the lower right side of this capillary. **C** and **D** show a capillary (asterisk) from a rat 1 day after pilocarpine-induced seizures. Note that the cell body of an astrocyte (a) lies adjacent to the basal lamina (black arrowheads in **D**) of this capillary. Bundles of intermediate filaments were observed in the cell body of this astrocyte. **E** and **F** show a reactive astrocyte (a) from a rat 5 days after pilocarpine-induced seizures. Note the large bundle of intermediate filaments filling its perikaryal cytoplasm. Scale bars for **A** and **E** = 2 um; for **B–D** and **F** = 1 μm.

cytoplasm with heterogeneously sized vacuoles (Fig. 6). The cell bodies of astrocytes within 10 μm of capillaries had processes that contained bundles of intermediate filaments and elongated mitochondria (Figs. 6A, 6B). In the preparations obtained from rats 1 day after pilocarpine-induced seizures, all of the capillaries examined in the hilus had cell bodies of astrocytes apposed to the basal lamina (Figs. 6C, 6D). These astrocytic cell bodies varied in the number and size of the bundles of glial filaments, and their contiguous astrocytic processes that apposed the basal lamina of capillaries also contained bundles of glial filaments (Figs. 6C, 6D). All these changes were also observed at each of the later time points analyzed in this study. In addition, astrocyte cell bodies examined at later time points had larger bundles of glial filaments (Figs. 6E, 6F), reflecting the classically described glial hypertrophy as observed in GFAP-labeled preparations of brain sections from epileptic rats (Hansen et al., 1990).

Discussion

The results from the current study show that the activation of astrocytes and microglial cells has a different spatial and temporal response to pilocarpine-induced seizures. These data will be discussed in the context of the cells' distinctive morphological patterns and features.

The results suggest that within 1 day after seizures, an early microglial response occurs in CA1, CA3, and the dentate gyrus. The fact that Iba1 immunoreactivity remains significantly elevated at 2 days after seizures coincides with the fact that the microglial activation is ongoing at this time point. It should be noted that the morphometric analysis confirmed the early microglial activation observed qualitatively, because the microglial cells were pleomorphic and at later time points appeared rod-like. The qualitative data also showed that the microglia remained in an activated state at least 3–5 days after the initial convulsive insult. The quantitative morphometric data supported this conclusion, revealing significant increases in total process area and an increased number of process endings indicative of more branching.

The results showing that S100-B immunolabeling is elevated beginning 1 day after the seizures in CA3 and continuing through day 3 where it is elevated in all of the regions examined reflects the role S100B plays in the neuroinflammatory response. Not only does S-100B stimulate the expression and release of the proinflammatory cytokine interleukin-6 (Li et al., 2000), but elevated S-100B is associated with microglial cells expressing interleukin1α (Sheng et al., 1997). Moreover, S100B inhibits intermediate filament assembly of GFAP (Ueda et al., 1994; Bianchi et al., 1996), and experimental reduction of S-100B results in fewer GFAP positive glial cells (Selinfreund et al., 1991). The increase in S100B shown here, beginning by 1 day and peaking at 3 days, may therefore be responsible for stimulating the proliferation of astrocytes. This would be consistent with a previous report showing a preferential increase in the proliferation of GFAP-expressing radial glia-like astrocytes at 3 days after kainate acid-induced seizures (Huttmann et al., 2003).

While the densitometric analysis of GFAP did not show any significant differences, the data might be misleading because astereological analysis of the number of astrocytes was not performed. Previous studies have reported that astrocytic cell death occurs following seizures (Borges et al., 2006). It is possible that no net difference was seen in the densitometric analysis because astrocyte hypertrophy of the surviving GFAP-labeled astrocytes compensated for the death of GFAP-labeled cells following pilocarpine-induced seizures. This glial hypertrophy was observed in the light microscopic preparations and was also shown convincingly in electron microscopic images obtained from the hilus at all of the time points examined. The appearance of hypertrophied processes with large bundles of glial filaments as early as one day after seizures would presumably be preceded by increased GFAP mRNA, which can be seen in some regions of the hippocampus as early as 1.5 hrs after pilocarpine-induced seizures (Belluardo et al., 1996).

In the normal adult subgranular zone, the basement membrane of the capillaries is flanked by the traditional astrocytic endfeet (Cajal, 1911; Peters et al., 1991; Shapiro et al., 2005b). In the current study, by 1 day after seizures and continuing throughout the 5 days examined, the cell bodies of astrocytes appear adjacent to the capillaries, and their swollen astrocytic cytoplasm contains large bundles of intermediate filaments. In many cases, the cell body of the astrocyte is so closely apposed to the basement membrane (Fig. 6) that no classical astrocytic endfeet are present. This is consistent with similar findings at 30 days after pilocarpine-induced seizures (Shapiro et al., 2006).

Adult hippocampal neurogenesis has been shown to occur within an angiogenic niche, in close association with the capillaries and the astrocytes (Palmer et al., 2000). Hippocampal neurogenesis is altered at both short (Shapiro et al., 2007a) and long (Parent et al., 1997) time points after pilocarpine-induced seizures, and this alteration may be detrimental to the epileptic brain (Parent et al., 1997). It is possible that seizure-induced alterations to the angiogenic niche, such as a disruption of the blood-brain barrier (Bolwig et al., 1977; Petito et al., 1977) or altered astrocyte buffering potential (Bordey & Sontheimer, 1998), might underlie the seizure-induced alterations in hippocampal neurogenesis. Kang et al., (2006) have shown that astrocyte and microglial responses to pilocarpine-induced seizures in the dentate gyrus precede neuronal damage and are related to abnormal neurotransmission. Thus, controlling the rapid astrocytic and microglial response to seizures might limit the detrimental effects of seizure-induced neuroplasticity and neurodegeneration, which could potentially enhance the clinical efficacy of existing seizure therapy.

ACKNOWLEDGMENTS

The authors would like to recognize Dr. Zhiyin Shan for technical expertise and Dr. Devin Binder for meaningful discussions regarding a draft of this manuscript. We also acknowledge support from NIH grant R01-NS38331 (to CER).

We confirm that we have read the Journal's position on issues involved in ethical publication and affirm that this report is consistent with those guidelines.

Conflict of interest: There are no conflicts of interests for the authors of this paper.

REFERENCES

Austin JE, Buckmaster PS. (2004) Recurrent excitation of granule cells with basal dendrites and low interneuron density and inhibitory postsynaptic current frequency in the dentate gyrus of macaque monkeys. *J Comp Neurol* 476:205–218.

Belluardo N, Mudo G, Jiang XH, Condorelli DF. (1996) Induction of astroglial gene expression by experimental seizures in the rat: spatiotemporal patterns of the early stages *Glia* 16:174–186.

Bendotti C, Guglielmetti F, Tortarolo M, Samanin R, Hirst WD. (2000) Differential expression of S100beta and glial fibrillary acidic protein in the hippocampus after kainic acid-induced lesions and mossy fiber sprouting in adult rat. *Exp Neurol* 161:317–329.

Bianchi R, Garbuglia M, Verzini M, Giambanco I, Ivanenkov VV, Dimlich RVW, Jamieson GA Jr., Donato R. (1996) S100 (and β)-binding peptide (TRTK-12) blocks S100/GFAP interaction: identification of a putative S100 target epitope within the head domain of GFAP. *Biochim Biophys Acta* 1313:258–267.

Binder DK, Steinhäuser C. (2006) Functional changes in astroglial cells in epilepsy. *Glia* 54:358–368.

Bolwig TG, Hertz MM, Holm-Jensen J. (1977) Blood-brain barrier during electroshock seizures in the rat. *Eur J Clin Invest* 7:95–100.

Bordey A, Sontheimer H. (1998) Properties of human glial cells associated with epileptic seizure foci. *Epilepsy Res* 32:286–303.

Borges K, Gearing M, McDermott DL, Smith AB, Almonte AG, Wainer BH, Dingledine R. (2003) Neuronal and glial pathological changes during epileptogenesis in the mouse pilocarpine model. *Exp Neurol* 182:21–34.

Borges K, McDermott D, Irier H, Smith Y, Dingledine R. (2006) Degeneration and proliferation of astrocytes in the mouse dentate gyrus after pilocarpine-induced status epilepticus. *Exp Neurol* 201:416–427.

Briellmann RS, Kalnins RM, Berkovic SF, Jackson GD. (2002) Hippocampal pathology in refractory temporal lobe epilepsy: T2-weighted signal change reflects dentate gliosis. *Neurology* 58:265–271.

Buckmaster PS, Zhang GF, Yamawaki R. (2002) Axon sprouting in a model of temporal lobe epilepsy creates a predominantly excitatory feedback circuit. *J Neurosci* 22:6650–6658.

Cajal SR. (1911) *Histologie du Systeme Nerveux de l'Homme et des Vertebres, Vol. 2*. Maloine, Paris.

Drage MG, Holmes GL, Seyfried TN. (2002) Hippocampal neurons and glia in epileptic EL mice. *J Neurocytol* 31:681–692.

Garzillo CL, Mello LE. (2002) Characterization of reactive astrocytes in the chronic phase of the pilocarpine model of epilepsy. *Epilepsia* 43(Suppl 5):107–109.

Griffin WST, Stanley LC, Ling C, White L, Macleod V, Perrot LJ, White CL 3rd, Araoz C. (1989) Brain interleukin 1 and S-100 immunoreactivity are elevated in Down syndrome and Alzheimer's disease. *Proc Nat'l Acad Sci USA* 86:7611–7615.

Griffin WST, Yeralan O, Sheng JG, Boop FA, Mrak RE, Rovnaghi CR, Burnett BA, Feokistova A, Van Eldik LJ. (1995) Overexpression of the neurotrophic cytokine S100 beta in human temporal lobe epilepsy. *J Neurochem* 65:228–233.

Hansen A, Jorgensen OS, Bolwig TG, Barry DI. (1990) Hippocampal kindling alters the concentration of glial fibrillary acidic protein and other marker proteins in rat brain. *Brain Res* 531:307–311.

Huttmann K, Sadgrove M, Wallraff A, Hinterkeuser S, Kirchhoff F, Steinhäuser C, Gray WP. (2003) Seizures preferentially stimulate proliferation of radial glia-like astrocytes in the adult dentate gyrus: functional and immunocytochemical analysis. *Eur J Neurosci* 18:2769–2778.

Kang TC, Kim DS, Kwak SE, Kim JE, Won MH, Kim DW, Choi SY, Kwon OS. (2006) Epileptogenic roles of astroglial death and regeneration in the dentate gyrus of experimental temporal lobe epilepsy. *Glia* 54:258–271.

Li Y, Barger SW, Liu L, Mrak RE, Griffin WST. (2000) S100β induction of the proinflammatory cytokine interleukin-6 in neurons. *J Neurochem* 74:143–150.

McCloskey DP, Hintz TM, Pierce JP, Scharfman HE. (2006) Stereological methods reveal the robust size and stability of ectopic hilar granule cells after pilocarpine-induced status epilepticus in the adult rat. *Eur J Neurosci* 24:2203–2210.

Mello LE, Cavalheiro EA, Tan AM, Kupfer WR, Pretorius JK, Babb TL, Finch DM. (1993) Circuit mechanisms of seizures in the pilocarpine model of chronic epilepsy: cell loss and mossy fiber sprouting. *Epilepsia* 34:985–995.

Niquet J, Ben-Ari Y, Represa A. (1994) Glial reaction after seizure induced hippocampal lesion: immunohistochemical characterization of proliferating glial cells. *J Neurocytol* 23:641–656.

Palmer TD, Willhoite AR, Gage FH. (2000) Vascular niche for adult hippocampal neurogenesis. *J Comp Neurol* 425:479–494.

Parent JM, Yu TW, Leibowitz RT, Geschwind DH, Sloviter RS, Lowenstein DH. (1997) Dentate granule cell neurogenesis is increased by seizures and contributes to aberrant network reorganization in the adult rat hippocampus. *J Neurosci* 17:3727–3738.

Peters A, Palay SL, Webster H de F. (1991) *The fine structure of the nervous system: Neurons and their supporting cells*, 3rd Ed, Oxford University Press, New York.

Petito CK, Schaefer JA, Plum F. (1977) Ultrastructural characteristics of the brain and blood-brain barrier in experimental seizures. *Brain Res* 127:251–267.

Ribak CE, Tran PH, Spigelman I, Okazaki MM, Nadler JV. (2000) Status epilepticus-induced hilar basal dendrites on rodent granule cells contribute to recurrent excitatory circuitry. *J Comp Neurol* 428:240–253.

Rothermundt M, Peters M, Prehn JH, Arolt V. (2003) S100B in brain damage and neurodegeneration. *Micros Res Tech* 60:614–632.

Selinfreund RH, Barger SW, Pledger WJ, Van Eldik LJ. (1991) Neurotrophic protein S100β stimulates glial cell proliferation. *Proc Nat'l Acad Sci USA* 88:3554–3558.

Shapiro LA, Korn MJ, Ribak CE. (2005a) Newly generated dentate granule cells from epileptic rats exhibit elongated hilar basal dendrites that align along GFAP-immunolabeled processes. *Neuroscience* 136:823–831.

Shapiro LA, Korn MJ, Shan Z, Ribak CE. (2005b) GFAP-expressing radial glia-like cell bodies are involved in a one-to-one relationship with doublecortin-immunolabeled newborn neurons in the adult dentate gyrus. *Brain Res* 1040:81–91.

Shapiro LA, Ribak CE. (2006) Newly born dentate granule neurons after pilocarpine-induced epilepsy have hilar basal dendrites with immature synapses. *Epilepsy Res* 69:53–66.

Shapiro LA, Figueroa-Aragon S, Ribak CE. (2007a) Newly generated granule cells show rapid neuroplastic changes in the adult rat dentate gyrus during the first five days following pilocarpine-induced seizures. *Eur J Neurosci* 26:583–592.

Shapiro LA, Ng KL, Zhou QY, Ribak CE (2007b) Olfactory enrichment enhances the survival of newly born cortical neurons in adult mice. *NeuroReport* 18:981–985.

Sheng JG, Mrak RE, Griffin WST. (1997) Glial-neuronal interactions in Alzheimer's disease: progressive association of IL-1A+ microglial and S100β+ astrocytes with neurofibrillary tangle stage. *J Neuropath Exp Neurol* 56:285–290.

Ueda S, Gu XF, Whitaker-Azmitia PM, Naruse I, Azmitia EC. (1994) Neuro-glial neurotrophic interaction in the S-100 beta retarded mutant mouse (Polydactyly Nagoya). I. Immunocytochemical and neurochemical studies. *Brain Res* 633:275–283.

Vessal M, Dugani CB, Solomon DA, McIntyre Burnham W, Ivy GO. (2005) Might astrocytes play a role in maintaining the seizure-prone state? *Brain Res* 1044:190–196.

Yan SD, Chen X, Fu J, Chen M, Zhu H, Roher A, Slattery T, Zhao L, Nagashima M, Morser J, Migheli A, Nawroth P, Stern D, Schmidt AM. (1996) RAGE and amyloid-beta peptide neurotoxicity in Alzheimer's disease. *Nature* 382:685–691.